Supplementary Information for "Digital instability of a confined elastic meniscus" by Biggins et al.

May 22, 2013

1 Movies

The enclosed movies show the formation of the instability and our ability to pattern it in the bistable regime.

Movie1:

Typical experiment for a gap $a = 3.05mm$, showing a sinusoidal destabilization just before the sudden nucleation of a finger. Dimension of slab $29 \times 20mm$. The movie is slowed down by a factor of 20.

Movie2:

Movie showing the reversibility of the instability and its hysteretic character. The transient domain is relatively small compared to the size of a finger. Gap $a = 3.04mm$. Dimension of slab $13 \times 19mm$. Real speed.

Movie3:

Movie showing that identical fingering occurs even when the air-elastomer interface is replaced by an air-oil interface. The change in interfacial tension does not change either the onset of the instability or its wavelength, suggesting that the effects of interfacial tension are unimportant at leading order in determining this phenomenon.

Movie4:

Movie showing the possibility to nucleate a finger wherever along the front in the hysteretic region, when the two plates have been separated by a distance $\Delta z = 0.36mm$. The needle used to poke the gel is made of hydrophobic plastic. Gap $a = 3.04mm$. Dimension of slab $27 \times 19mm$. Real speed.

2 Theoretical model

Our two-dimensional elastic model of the instability successfully predicts the wavelength and threshold without any fitting parameters. Here, we provide further details of the theory associated with the calculations of the thickness integral of the energy and the stability analysis of the model.

We recall that we are modeling an elastic solid initially occupying the region of space $-\infty < x < \infty$, $0 < y < l$, $-a/2 < z < a/2$ where $a << l$ and which is perfectly adhered to rigid glass plates at $z = \pm a/2$. The glass plates are then moved further apart by an amount Δz so that they are at $z = \pm(a + \Delta z)/2$ and we seek to understand the response of the elastomer to this loading.

2.1 Quadratic form of the displacement and deformation gradient (eqns. (1) and (2))

The displacement of a point in the elastomer initially at (x, y, z) is $\mathbf{U}(x, y, z)$. Taking advantage of the thinness of the elastomer, we Taylor expand this displacement to quadratic order in z giving

$$\mathbf{U}(x, y, z) = \mathbf{A}(x, y) + z\mathbf{B}(x, y) + z^2\mathbf{C}(x, y) + ... \tag{S.1}$$

Imposing symmetry about $z = 0$ we see that $\mathbf{B}$ lies in the $\hat{\mathbf{z}}$ direction while $\mathbf{A}$ and $\mathbf{C}$ lie in the $x - y$ plane. Requiring that $\mathbf{U}(x, y, \pm a/2) = \pm\Delta z\hat{\mathbf{z}}/2$ so that the displacement on the boundaries matches that of the plates, we see that $\mathbf{B} = \Delta z\hat{\mathbf{z}}/a$ and that $\mathbf{A} = -(a^2/4)\mathbf{C}$. Since $\mathbf{A}$ is the displacement of a point in the $z = 0$ plane and lies entirely in the $z = 0$ plane, we write $\mathbf{A} = \mathbf{u}$ so the entire displacement becomes

$$\mathbf{U}(x, y, z) = (1 - 4z^2/a^2)\mathbf{u}(x, y) + (z\Delta z/a)\hat{\mathbf{z}}, \tag{S.2}$$

which corresponds to eqn. (1) in the article.

The deformation gradient F is defined as $F_{ij} = \delta_{ij} + \partial_j U_i$. Using ∇ as the in-plane gradient operator (i.e. $\nabla = \hat{\mathbf{x}}\frac{\partial}{\partial x} + \hat{\mathbf{y}}\frac{\partial}{\partial y}$) and I as the in-plane identity ($I = \hat{\mathbf{x}}\hat{\mathbf{x}} + \hat{\mathbf{y}}\hat{\mathbf{y}}$) we can evaluate F as

$$F = I + (1 - 4z^2/a^2)\nabla\mathbf{u} - 8z\mathbf{u}\hat{\mathbf{z}}/a^2 + (1 + \Delta z/a)\hat{\mathbf{z}}\hat{\mathbf{z}}, \tag{S.3}$$

which is eqn. (2) in the article.

Working in an $x-y-z$ basis and breaking $\mathbf{u}$ into components as $\mathbf{u} = u_x\hat{\mathbf{x}} + u_y\hat{\mathbf{y}}$ we can write F explicitly as

$$F = \begin{pmatrix} 1+(1-\frac{4z^2}{a^2})\frac{\partial u_x}{\partial x} & (1-\frac{4z^2}{a^2})\frac{\partial u_x}{\partial y} & -\frac{8zu_x}{a^2} \\ (1-\frac{4z^2}{a^2})\frac{\partial u_y}{\partial x} & 1+(1-\frac{4z^2}{a^2})\frac{\partial u_y}{\partial y} & -\frac{8zu_y}{a^2} \\ 0 & 0 & 1+\Delta z/a \end{pmatrix}. \tag{S.4}$$

2.2 2-D Energy Function (eqn. (3))

We write our two dimensional elastic energy as

$$L(\mathbf{u}, P) = \mu \int_{-a/2}^{a/2} \tfrac{1}{2}\mathrm{Tr}\left(F.F^T\right) - \frac{P(x,y)(\mathrm{Det}(F)-1)}{1+\Delta z/a}\mathrm{d}z, \tag{S.5}$$

where the first term is a standard neo-hookean energy density for a deformed elastomer, and the second term models the elastomers incompressibility by imposing thickness averaged incompressibility at every point in the $x-y$ plane via a pressure-like Lagrange multiplier field $P(x,y)$. The coefficient of this term is simply for algebraic convenience. Evaluating the first term in this integral is a simple matter of expanding $\mathrm{Tr}\left(F.F^T\right)$ and integrating each term separately:

$$\begin{aligned} &\mathrm{Tr}\left(FF^T\right) = 2 + (1-4z^2/a^2)^2\mathrm{Tr}\left(\nabla\mathbf{u}(\nabla\mathbf{u})^T\right) + \\ &64z^2\mathbf{u}\cdot\mathbf{u}/a^4 + (1+\Delta z/a)^2 + 2(1-4z^2/a^2)\nabla\cdot\mathbf{u} \end{aligned} \tag{S.6}$$

$$\begin{aligned} \int_{-a/2}^{a/2} \mathrm{Tr}\left(F.F^T\right)\mathrm{d}z &= a(2+(1+\Delta z/a)^2) + \frac{4a}{3}\nabla\cdot\mathbf{u} \\ &\quad + \frac{8a}{15}\mathrm{Tr}\left(\nabla\mathbf{u}(\nabla\mathbf{u})^T\right) + \frac{16}{3a}\mathbf{u}\cdot\mathbf{u} \qquad \text{(S.7)} \\ &= \frac{5a}{6}\mathrm{Tr}\left(G.G^T\right) + \frac{16}{3a}\mathbf{u}\cdot\mathbf{u} + \mathrm{const} \qquad \text{(S.8)} \end{aligned}$$

In the last line we have introduced an effective two dimensional deformation gradient $G = I + \frac{4}{5}\nabla\mathbf{u}$.

The second term in the energy can be treated in a similar way. We first note that $\mathrm{Det}(F) = (1+\Delta z/a)\mathrm{Det}\big(I + (1-4z^2/a^2)\nabla\mathbf{u}\big)$. Secondly, we use the (two-dimensional) relation that $\mathrm{Det}(I+cB) = 1 + c\mathrm{Tr}\,(B) + c^2\mathrm{Det}(B)$

to expand $\mathrm{Det}(F)$ then integrate each term separately giving:

$$\begin{aligned}\int_{-a/2}^{a/2} \mathrm{Det}(F)\,\mathrm{d}z =& a\left(1+\frac{\Delta z}{a}\right) \\ &\times\left(1+\frac{2}{3}\mathrm{Tr}\left(\nabla\mathbf{u}\right)+\frac{8}{15}\mathrm{Det}(\nabla\mathbf{u})\right).\end{aligned} \tag{S.9}$$

Applying the same identity, this can be rewritten as $a(1+\Delta z/a)(5\mathrm{Det}(G)+1)/6$. Assembling these two results, we can write the entire integrated energy as

$$\begin{aligned}L =& \frac{5\mu a}{6}\left(\frac{1}{2}\mathrm{Tr}\left(G.G^T\right)+\frac{16}{5}\frac{\mathbf{u}\cdot\mathbf{u}}{a^2}\right. \\ &\left.-P\left(\mathrm{Det}(G)-1+\frac{6\Delta z}{5(a+\Delta z)}\right)+\mathrm{const}\right).\end{aligned} \tag{S.10}$$

Finally, we neglect the constant, drop the pre-factor and, since $\Delta z_t \sim a^2/l << l$, replace $\Delta z/(a+\Delta z)$ by $\Delta z/a$, to write

$$L \propto \tfrac{1}{2}\mathrm{Tr}\left(G.G^T\right)+\tfrac{16}{5}|\mathbf{u}/a|^2-P\left(\mathrm{Det}(G)-1+\tfrac{6}{5}\Delta z/a\right),$$

which corresponds to eqn. (3) in the main article.

2.3 Bulk equations and boundary conditions (eqns. (4)-(5))

We now seek to minimize the total energy of the elastomer, so we find the Euler-Lagrange equations for $\mathbf{u}$ and P:

$$\partial_j\frac{\partial L}{\partial\partial_j u_i}=\frac{\partial L}{\partial u_i} \tag{S.11}$$

$$\frac{\partial L}{\partial P}=0 \tag{S.12}$$

The second of these straightforwardly evaluates to give

$$\mathrm{Det}(G)=1-\tfrac{6}{5}\Delta z/a. \tag{S.13}$$

The right-hand side of the first equation is also straightforward: $\partial L/\partial u_i = (5\mu a/6)(32/5)u_i/a^2$. The left-hand side can be evaluated using the result that $\partial\mathrm{Det}(A)/\partial A_{ij}=\mathrm{Det}(A)\,A^{-T}_{ij}$, so we have

$$\frac{\partial L}{\partial\partial_j u_i}=\frac{5\mu a}{6}\left(\tfrac{4}{5}G_{ij}-\tfrac{4}{5}P\mathrm{Det}(G)\,G^{-T}_{ij}\right). \tag{S.14}$$

To construct the whole equation we need one final result, $\partial_j \mathrm{Det}(G)\, G^{-T}_{ij} = 0$, which is easily seen by explicitly writing out G. We can then write the entire equation as

$$\tfrac{4}{5} a^2 \nabla^2 \mathbf{u} - \mathrm{Det}(G)\, G^{-T} \cdot a^2 \nabla P = 8\mathbf{u}. \tag{S.15}$$

Equations S.15 and S.13 correspond to eqn. (4) in the main article.

Since our problem does not impose any additional constraints at $y = 0, l$ we take the natural boundary conditions, corresponding to an unconstrained minimization of the energy, given by $\frac{\partial L}{\partial \partial_j u_i} \hat{n}_j = 0$ where $\hat{\mathbf{n}}$ is the unit normal vector at the boundary. In our case $\hat{\mathbf{n}} = \hat{\mathbf{y}}$ on both boundaries. We have already evaluated this derivative, so we can immediately write the boundary condition as

$$\left(G - P\mathrm{Det}(G)\, G^{-T}\right) \cdot \hat{\mathbf{y}} = 0. \tag{S.16}$$

corresponding to eqn. (5) in the main article.

2.4 Solving the model (eqns. (6) to (14))

To solve our model, we introduce a trial form for the solutions consisting of a large translationally invariant part and an infinitesimal oscillatory part:

$$\mathbf{u} = Y_1(y)\hat{\mathbf{y}} + \epsilon \cos(kx) Y_2(y)\hat{\mathbf{y}} + \epsilon \sin(kx) X_2(y)\hat{\mathbf{x}} \tag{S.17}$$

$$P = 1 + P_1(y) + \epsilon \cos(kx) P_2(y). \tag{S.18}$$

The translationally invariant part corresponds to the deformations before the fingering instability, which we call the base-state. Working in the $x - y$ coordinate system we have

$$G_1 = \begin{pmatrix} 1 & 0 \\ 0 & 1 + \frac{4}{5} Y_1'(y) \end{pmatrix}, \tag{S.19}$$

and

$$\mathrm{Det}(G_1)\, G_1^{-T} = \begin{pmatrix} 1 + \frac{4}{5} Y_1'(y) & 0 \\ 0 & 1 \end{pmatrix}. \tag{S.20}$$

Substituting G_1 into eqn. S.13 we get

$$\tfrac{4}{5} Y_1'(y) = -\tfrac{6}{5} \Delta z / a, \tag{S.21}$$

which we can solve for Y_1 to get

$$Y_1(y) = \frac{3\Delta z (l - 2y)}{4a}, \tag{S.22}$$

in which we have fixed the constant on integration by requiring that $Y_1(l/2) = 0$ to preserve the symmetry about $y = l/2$. This corresponds to eqn. (8) in the main article. Since $\nabla P = P_1'(y)\hat{\mathbf{y}}$, we can write eqn. S.15 as

$$\tfrac{4}{5}a^2 Y_1''(y) - a^2 P_1'(y) = 8Y_1(y). \tag{S.23}$$

This can be integrated to find

$$P_1(y) = 6y\Delta z(y-l)/a^3 - \tfrac{6}{5}\Delta z/a. \tag{S.24}$$

This corresponds to eqn. (9) in the main article. The constant of integration has been found by applying the boundary condition (eqn. S.16) which reads:

$$(\tfrac{4}{5}Y_1'(y) - P_1(y))\big|_{y=0,l} = 0. \tag{S.25}$$

We consider adding an infinitesimal oscillatory perturbation to the base-state to examine its stability. We now have

$$G = G_1 + \frac{4\epsilon}{5}\begin{pmatrix} k\cos(kx)X_2(y) & \sin(kx)X_2'(y) \\ -k\sin(kx)Y_2(y) & \cos(kx)Y_2'(y) \end{pmatrix}, \tag{S.26}$$

$$\begin{aligned}\mathrm{Det}(G)\,G^{-T} &= \mathrm{Det}(G_1)\,G_1^{-T} \\ &+ \frac{4\epsilon}{5}\begin{pmatrix} \cos(kx)Y_2'(y) & k\sin(kx)Y_2(y) \\ -\sin(kx)X_2'(y) & k\cos(kx)X_2(y) \end{pmatrix}.\end{aligned} \tag{S.27}$$

Substituting G into eqn. S.13 and expanding to first (linear) order in ϵ gives

$$\epsilon\cos(kx)((1+\tfrac{4}{5}Y_1'(y))kX_2(y) + Y_2'(y)) = 0 \tag{S.28}$$

Recalling the form of $Y_1(y)$ we see that

$$Y_1'(y) = -\frac{3\Delta z}{2a}. \tag{S.29}$$

We expect the threshold value of Δz to scale as $\Delta z_t \sim a^2/l$ so, in the limit of $a << l$, we expect $\Delta z_t << a$ and hence $Y_1'(y) << 1$. This means we can neglect $Y_1'(y)$ in the above equation, so the solution for $X_2(y)$ is simply

$$X_2(y) = -Y_2'(y)/k. \tag{S.30}$$

We can also write ∇P as

$$\nabla P = \begin{pmatrix} -\epsilon k\sin(kx)P_2(y) \\ P_1'(y) + \epsilon P_2'(y)\cos(kx) \end{pmatrix}, \tag{S.31}$$

so the x component of eqn. S.15 is, to linear order in ϵ,

$$\begin{aligned}&\tfrac{4}{5}a^2(X_2''(y) - k^2X_2(y)) \\ &\quad + a^2((1+\tfrac{4}{5}Y_1'(y))kP_2(y) - \tfrac{4}{5}kY_2(y)P_1'(y)) = 8X_2(y)\end{aligned} \tag{S.32}$$

We can again neglect $Y_1'(y) << 1$ term so, substituting in our solution for $X_2(y)$, we can solve for algebraically for P_2 to get

$$P_2(y) = \frac{4}{5}\left(Y_2(y)P_1'(y) - \left(1 + \frac{10}{a^2k^2}\right)Y_2'(y) + \frac{Y_2'''(y)}{k^2}\right). \tag{S.33}$$

Finally, we can evaluate the y component of eqn. S.15 to linear order in ϵ to get

$$\begin{aligned}\tfrac{4}{5}a^2(Y_2''(y) - k^2Y_2(y)) - a^2(P_2'(y) + \tfrac{4}{5}kX_2(y)P_1'(y)) \\ = 8Y_2(y).\end{aligned} \tag{S.34}$$

Substituting in our results for $X_2(y)$ and $P_2(y)$ gives

$$\begin{aligned}k^2Y_2(y)\left(10 + a^2k^2 + a^2P_1''(y)\right) + a^2Y_2^{(4)}(y) \\ = 2\left(5 + a^2k^2\right)Y_2''(y).\end{aligned} \tag{S.35}$$

Recalling the form of P_1, we see that

$$a^2P_1''(y) = 12\Delta z/a \tag{S.36}$$

so, as with $Y_1'(y)$, we see that $a^2P_1''(y) << 1$ when $a << l$ so we can ignore $P_1''(y)$ in the above equation giving

$$\begin{aligned}a^2k^2Y_2(y)\left(10 + a^2k^2\right) + a^4Y_2^{(4)}(y) \\ = 2\left(5 + a^2k^2\right)a^2Y_2''(y),\end{aligned} \tag{S.37}$$

which corresponds to eqn. (10) in the main article. We focus on the boundary at $y = 0$ and so look for solutions that decay as $y \to \infty$. We write Y_2 as a linear sum of the two such solutions

$$Y_2 = c_1 \exp\left(-\sqrt{10/a^2 + k^2}y\right) + c_2 \exp\left(-ky\right), \tag{S.38}$$

which is equation (11) in the main article.

We impose the boundary condition at $y = 0$. Since these solutions decay as $y \to \infty$ we can neglect the boundary condition at $y = l$. The linear correction to the boundary condition at $y = 0$ (eqn. S.16) is

$$\frac{4}{5}\begin{pmatrix} X_2'(0) \\ Y_2'(0)\end{pmatrix} = P_2(0)\begin{pmatrix} 0 \\ 1\end{pmatrix} + (1 + P_1(0))\begin{pmatrix} \frac{4}{5}kY_2(0) \\ \frac{4}{5}kX_2(0)\end{pmatrix}. \tag{S.39}$$

However, $P_1(0) = -\frac{6}{5}\Delta z/a \to 0$ when $a << l$ so the x component, after substituting for X_2, is

$$-Y_2''(0) = k^2 Y_2(0). \tag{S.40}$$

Substituting in our result for Y_2 we solve for c_2 to get

$$c_1 = -c_2 \frac{a^2k^2}{5 + a^2k^2}. \tag{S.41}$$

The y component requires us to evaluate $P_2(0)$. To do this we first note that

$$-\left(1 + \frac{10}{a^2k^2}\right) Y_2'(0) + \frac{Y_2'''(0)}{k^2} = \frac{10c_2}{a^2k}, \tag{S.42}$$

and secondly that $P_1'(0) = -6l\Delta z/a^3$, which does not vanish for $a << l$ because it contains a power of l. Assembling the entire boundary condition then gives

$$Y_2'(0) = -\frac{6l\Delta z}{a^3} Y_2(0) + \frac{10c_2}{a^2k} - Y_2'(0), \tag{S.43}$$

which, upon substituting for Y_2 and c_1 and solving algebraically for Δz_t gives

$$\Delta z_t = \frac{a^2}{l} \frac{25 + a^2k^2\left(10 + ak\left(ak - \sqrt{10 + a^2k^2}\right)\right)}{15ak} \tag{S.44}$$

which corresponds to eqn. (12) in the main article. This result tells us the threshold Δz at which a mode with wave-number k becomes unstable. We find the first unstable mode by minimizing this result over k, to predict that the first unstable mode has

$$\lambda \approx 2.74...a \tag{S.45}$$

$$\Delta z_t \approx 1.69...a^2/l. \tag{S.46}$$

which correspond to equations (13)-(14) in the main article.

3 Numerical Simulations

All simulations were performed using the commercial finite element software ABAQUS 6.11. A sketch of the simulation domain is shown in Fig. S.1. Although the transition under examination is purely elastic, its subcritical nature means that it cannot be simulated using equilibrium methods, so instead we use Newtonian dynamics with both numerical and viscous damping. We ran two types of simulations: lower resolution simulations

with many wavelengths to capture the behavior at onset and high resolution simulations focusing on a single digit to capture the profile of the fingers.

1. Material properties

   The gel is modeled as an incompressible neo Hookean material with shear modulus of $500Pa$ and a density $10^3\text{Kg}/m^3$. We used a large Rayleigh damping model to ensure that the system is overdamped. For a given mode i the fraction of critical damping, ξ_i, can be expressed in terms of the damping factors α_R and β_R as:

   $$\xi_i = \frac{\alpha_R}{2\omega_i} + \frac{\beta_R \omega_i}{2}, \tag{S.47}$$

   where ω_i is the natural frequency at this mode, α_R is for mass proportional damping and β_R is for stiffness proportional damping. To define Rayleigh damping, we need to specify α_R and β_R. We load the boundary near the critical displacement and perform a linear perturbation procedure to extract ω_i, $i = 1$ to 5, and correspondingly specify α_R to make ξ_i around 5. This is only a crude estimation of the damping coefficient as the stiffness matrix is a function of strain. When the fingers are fully grown, we expect the natural frequency is different from that of the onset state. After a try and error, we set $\alpha_R = 8000$ to 10000 to damp out the lowest frequency oscillation. For the highest frequency, we rely on numerical damping (which will be documented later) and set $\beta_R = 0$.

2. Boundary conditions

   Symmetric boundary conditions are applied on the two lateral planes (highlighted in yellow), the middle plane (light grey), and the back plane (blue). Therefore only a quarter of the physical thin slab is simulated to save computational power. The front surface (green) is stress free and Gaussian white noise is applied on its initial y coordinate in order to trigger the instability at the critical loading displacement. The mean magnitude of the noise is 2% of the smallest mesh size inside the system. The top surface is pulled apart at such a small constant velocity that it always takes 5 to 10 minutes before the top surface is loaded up to the critical displacement. Once oscillations of the front surface ore detected., the pulling is stopped and the top surface is held still while the system evolves freely.

3. Meshes and elements

   First, to get the displacement and wavelength of the onset of the instability, we run the simulation in a long cell (which contains 8 to 9 wavelengths) containing 401 nodes for the length, 76 nodes for the half-width and 26 nodes for the half-gap. This is more than adequate to detect the point of onset and the wavelength of the unstable mode, but, as the fingers grow, the strain at the tip of the fingers becomes very large (greater than 7) so we need a finer mesh. In order to capture the profile of the fully grown finger, we set the length of gel slab as half the previously calculated wavelength, and keep the boundary conditions the same. We use $201 \times 76 \times 26$ nodes to a quarter of a single finger, which is sufficient to resolve its full profile, even with the very large strains at its tip. Mesh density is geometrically biased towards the free front and middle plane, where the nonlinearity is the most pronounced after instability happens. C3D8H (8-node linear brick, hybrid with constant pressure) elements are adopted. The pressure penalty serves as an additional degree of freedom to ensure the constraint of incompressibility.

4. Time integrator

   As the material is incompressible, it is impossible to simulate the dynamic response with an explicit method as the stable time increment would be inversely proportional to the bulk modulus. Therefore we use an implicit method. Both the Hilber-Hughes-Taylor (HHT) integrator and backward Euler integrator gave the same onset of instability and fastest growing mode. In our system, we did not resolve the high-frequency vibrations and used a large numerical dissipation to obtain convergence during the loading history. In the HHT scheme, we choose $\alpha = -1/3$, $\beta = 1/4(1-\alpha)^2$ and $\gamma = 1/2 - \alpha$ to achieve the maximum numerical damping [1] with an adaptive time step which is reduced in the neighborhood of instability.

5. Dimensions of the samples

   We choose layer dimensions to ensure that the ratio of the width to the gap thickness is large (over 10) so that the layer can reasonably be thought of as thin. Our choice of length containing 8-9 wavelengths was determined to keep a low overhead on the computational costs. We note that this causes some end-effects in our simulation, which explains why the calculated wavelength is slightly below our experimentally observed wavelength. Tab. 1 shows the sample dimensions used, while

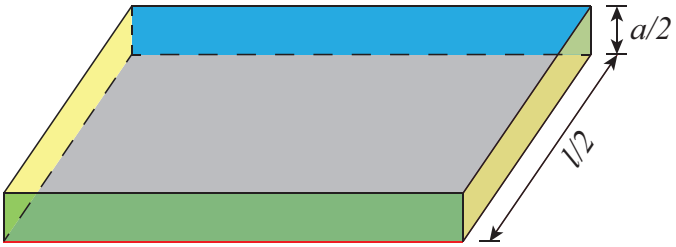

Figure S.1: Sketch of the simulation domain. Only a quarter of the thin slab is simulated. To detect whether the front surface (green) is oscillatory, we extract the displacement at the intersection line (red) where the middle plan (light grey) and front surface meet.

Table 1: Sample Dimensions (mm)

length	10	20	30	40	50	60	70	80	100.2	149
width	40	40	40	40	60	60	80	80	58.5	55.8
gap thickness	0.5	1.0	1.5	2.0	2.5	3.0	3.5	4.0	5.04	7.45

Fig. S.2 shows the $3D$ geometry of the fully grown finger right after the instability. Only one finger with periodic boundary conditions was actually simulated.

References

[1] Hilber, H. M., T. J. R. Hughes, and R. L. Taylor, Improved Numerical Dissipation for Time Integration Algorithms in Structural Dynamics, Earthquake Engineering and Structural Dynamics, vol. 5, pp. 283C292, 1977.

Figure S.2: $3D$ geometry of a single finger right after the instability. Only one finger was simulated with periodic boundary conditions. ADOBE READER allows for the manipulation of this interactive figure.